Will M. Bender and Udo Becker*

Resolving the kinetics of individual aqueous reaction steps of actinyl (AnO_2^+ and AnO_2^{2+}; An = U, Np, and Pu) tricarbonate complexes with ferrous iron and hydrogen sulfide from first principles

https://doi.org/10.1515/ract-2018-3083
Received November 27, 2018; accepted June 10, 2019; published online July 25, 2019

Abstract: The solubility and mobility of actinides (An), like uranium, neptunium, and plutonium, in the environment largely depends on their oxidation states. Actinyls ($An^{V,VI}O_2^{+/2+}{}_{(aq)}$) form strong complexes with available ligands, like carbonate (CO_3^{2-}), which may inhibit reduction to relatively insoluble $An^{IV}O_{2(s)}$. Here we use quantum-mechanical calculations to explore the kinetics of aqueous homogeneous reaction paths of actinyl tricarbonate complexes ($[AnO_2(CO_3)_3]^{5-/4-}$) with two different reductants, $[Fe(OH)_2(H_2O)_4]^0$ and $[H_2S(H_2O)_6]^0$. Energetically-favorable outer-sphere complexes (OSC) are found to form rapidly, on the order of milliseconds to seconds over a wide actinyl concentration range (pM to mM). The systems then encounter energy barriers (E_a), some of which are prohibitively high (>100 kJ/mol for some neptunyl and plutonyl reactions with Fe^{2+} and H_2S), that define the transition from outer- to inner-sphere complex (ISC; for example, calculated E_a of ISC formation between UO_2^+ and UO_2^{2+} with Fe^{2+} are 35 and 74 kJ/mol, respectively). In some reactions, multiple OSCs are observed that represent different hydrogen bonding networks between solvent molecules and carbonate. Even when forming ISCs, electron transfer to reduce An^{6+} and An^{5+} is not observed (no change in atomic spin values or lengthening of $An-O_{ax}$ bond distances). Proton transfer from bicarbonate and water to actinyl O was tested as a mechanism for electron transfer from Fe^{2+} to U^{6+} and Pu^{6+}. Not all proton transfer reactions yielded reduction of An^{6+} to An^{5+} and only a few pathways were energetically-favorable (e. g. H^+ transfer from H_2O to drive Pu^{6+} reduction to Pu^{5+} with $\Delta E = -5$ kJ/mol). The results suggest that the tricarbonate complex serves as an effective shield against actinide reduction in the tested reactions and will maintain actinyl solubility at elevated pH conditions. The results highlight reaction steps, such as inner-sphere complex formation and electron transfer, which may be rate-limiting. Thus, this study may serve as the basis for future research on how they can be catalyzed by a mineral surface in a heterogeneous process.

Keywords: Actinyl carbonate complex, quantum-mechanical calculations, reaction kinetics, redox reaction, environmental geochemistry.

1 Introduction

The chemistry of early actinide elements in the environment is a major concern with regards to the long-term storage of nuclear waste. Elements like uranium, neptunium, and plutonium are radioactive and pose a hazard to humans and other biota if released. These three elements assume a range of oxidation states (most commonly between +3 and +6) and can exist in a diverse array of solid and aqueous species [1]. In oxidizing environments, higher-valent forms of these actinides form the actinyl molecule with the formula AnO_2^{x+}. The molecular charges of +1 and +2 correspond to the penta- and hexavalent actinide oxidation states, respectively. These species are soluble and mobile under a range of solution conditions and form strong complexes with various inorganic and organic ligands [2–4]. These soluble forms of the actinides pose the greatest threat in terms of their ability to disperse radioactivity in the environment. The reduction of actinides to the +4 and +3 oxidation states, in most cases, results in the precipitation of insoluble oxide mineral phases (e. g. uraninite, $UO_{2(s)}$) [5]. Therefore, reactions of actinyls and their aqueous complexes with various reductants, including Fe^{2+} and H_2S, are of utmost concern when thinking of ways in which the mobility of these contaminants may be attenuated.

Some of the most stable and abundant actinide complexes in natural waters are the ones formed with carbonate (CO_3^{2-}) [6]. These complexes are expected to be the major forms of dissolved U, Np, and Pu in carbonate-bearing waters (e. g. seawater and limestone-hosted

***Corresponding author: Udo Becker,** Department of Earth and Environmental Sciences, University of Michigan, Room 2534, 1100 N University Ave, Ann Arbor, MI 48109-1005, USA, E-mail: ubecker@umich.edu
Will M. Bender: Department of Earth and Environmental Sciences, University of Michigan, Room 2534, 1100 N University Ave, Ann Arbor, MI 48109-1005, USA

groundwater) [6–8]. As such, the chemical behavior and reactions of these complexes are of particular interest. The thermodynamics of complex formation and the structure of U, Np, and Pu carbonate complexes has been explored in detail by experimental [9–13] and computational [14–16] approaches alike. From these efforts, it is clear that the actinyl tricarbonate complex, $[AnO_2(CO_3)_3]^{5-/4-}$, is the dominant form of uranyl, neptunyl, and plutonyl species at higher pH (>8) and moderate ionic strength [8, 13, 17]. The stability of these complexes is even harnessed in analytical settings when adsorbed or precipitated actinides species need to be desorbed or (re)dissolved for analysis [18–20]. Depending on the solution conditions, a number of other carbonate-bearing complexes are known to form as well, including those with just one or two carbonate ligands [13, 14] and tricarbonate complexes with counter-ions (e. g. Ca^{2+} in $[Ca_2AnO_2(CO_3)_3]^0$) [21, 22]. This study focuses on the tricarbonate complex without any counter ions. In this structure, each of the carbonate molecules assumes bidentate configuration and lays flat in an equatorial plane to produce a six-fold ring of $An–O_{carbonate}$ coordination. A representative calculated structure, that of $[UO_2(CO_3)_3]^{4-}$ is presented in Figure 1.

The aqueous redox chemistry of actinyls is an area of ongoing research. Many reactions are possible in solution (i. e. homogeneous reactions) or at mineral surfaces (i. e. heterogeneous reactions). Prior experimental and computational research has focused on the reactions of actinides with aqueous Fe^{2+} and Fe (oxyhydr)oxide mineral phases as these species constitute some of the most widespread reductants in natural and engineered environments where (corroding) steel may be present [23–25]. A smaller body of research has explored reactions with Fe sulfide minerals [26–29] and H_2S [30]. Reduction of actinides in solution has been shown to be possible, however, complete reduction of An^{6+} to An^{4+} is not observed in all cases, possibly due to large energy costs associated with alteration of the cation coordination environment between $An^{6+/5+}$ and An^{4+} [3, 7, 31, 32]. In some experiments, it has been observed that increasing the pH to 7 or above and/or carbonate concentration can dramatically decrease U^{6+} reduction to nearly zero in reactions with anthraquinone-2,6,-disulfonate (an organic reductant) [33], amorphous FeS [20], and zero-valent iron [34]. In addition, higher pH conditions drive desorption or maintain solubility of negatively-charged actinide complexes above the points of zero charge for many minerals [22, 35, 36]. This indicates that homogeneous reactions of these complexes are likely most important as controls on actinide mobility at alkaline pH conditions.

Investigation of the redox behavior of actinyl carbonate complexes has broadly found that carbonate complexation inhibits reduction, particularly when compared with redox reactions involving the $[AnO_2(H_2O)_5]^{+/2+}$ complex. This effect is made clear by comparing the reduction potentials in Equations 1 and 2, as measured via cyclic voltammetry [37] versus the Ag/AgCl reference electrode:

$$[UO_2(H_2O)_5]^{2+} + e^- \rightarrow [UO_2(H_2O)_5]^{+} \quad E_{1/2} = -0.169\ \text{V} \qquad (1)$$

$$[UO_2(CO_3)_3]^{4-} + e^- \rightarrow [UO_2(CO_3)_3]^{5-} \quad E_{1/2} = -0.820\ \text{V} \qquad (2)$$

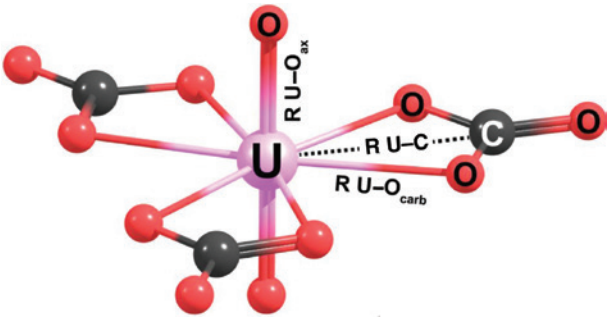


Figure 1: The calculated structure of $[UO_2(CO_3)_3]^{4-}$.
The three carbonate groups are in bidentate coordination of the central U^{6+} in the linear uranyl molecule. The $U–O_{ax}$ bond length (labeled as R), an indicator of oxidation state, is slightly longer than those found in uranyl water or hydroxide complexes. The $U–O_{carbonate}$ and U–C distances are also an important measure of the actinide valence in this configuration and all these distances increase if U^{6+} is reduced to U^{5+}. Analogous complexes and structural responses are observed for the complexes of neptunyl and plutonyl.

Clearly, the redox potential of the carbonate complex is significantly lower than that of the pentaquo complex. In this same study, rate constants (k^0) of heterogeneous electron transfer at the mercury drop electrode interface were found to be two orders of magnitude slower for the carbonate complex reaction versus that of the water complex ($k^0 = 2.6 \times 10^{-5}$ vs. 2.8×10^{-3} cm/s).

This study seeks to characterize the redox behavior and kinetics of complex formation between actinyl tricarbonate complexes of uranyl, neptunyl, and plutonyl with Fe^{2+} and H_2S to see how carbonate may protect these species from reduction and maintain actinide mobility and solubility in the environment. The results are compared to a computational study [38] of the reduction of uranyl tricarbonate by Fe^{2+} and various experimental findings [6, 22, 34, 35, 39, 40]. In addition, the computational methodology, previously employed to investigate the kinetics of

redox reactions of plutonyl hydrolysis complexes [41], is evaluated and reaction rates of aqueous complexes with and without carbonate ligands are compared. The results presented here elucidate which transition steps (outer-sphere complex formation vs. inner-sphere complex formation vs. electron transfer), are rate-limiting for homogeneous actinyl reduction and indicate which steps may be catalyzed by mineral surfaces. Such heterogeneous reactions of adsorbed species on mineral or colloid surfaces and acidic solution conditions, more readily able to facilitate proton transfer, are likely to be more favorable for actinyl reduction.

2 Computational methods

Quantum-mechanical calculations to optimize the atomic and electronic structures of the tested compounds were carried out using the Gaussian 09 (revision A.02) code [42]. The calculations were performed using the B3LYP hybrid density functional [43, 44] coupled with the LANL2DZ (for H, O, C, and S) [45–47] and Stuttgart relativistic small-core (for Fe, U, Np, and Pu) [48, 49] basis sets. This combination of basis set and hybrid functional has been shown to be effective and reliable in prior investigations of actinide chemistry [38, 50–52]. Corresponding pseudopotentials were used for S, U, Np, and Pu atoms to lessen computational expense. The S, Fe, and actinide pseudopotentials account for the contribution of 10, 10, and 60 (small core) inner shell electrons, respectively. The basis set and pseudopotential information was acquired from the EMSL Basis Set Library [53, 54].

To simulate an aqueous environment, a combination of explicit and implicit hydration approaches was used. The first coordination shell of Fe^{2+} and H_2S was modeled explicitly with six H_2O and/or OH^- in an octahedral arrangement. Hydroxide was used to balance the charge of the Fe^{2+} cation and minimize the electrostatic attraction to the negatively-charged actinyl tricarbonate complex and so that both reductant species would be charge-neutral. The net charge of the models was either −4 or −5 depending on the charge of actinyl carbonate complex. The unpaired spins on actinides (in a high spin configuration Pu^{4+} = 4 unpaired e^-; Np^{4+}, Pu^{5+} = 3 unpaired e^-; U^{4+}, Np^{5+}, Pu^{6+} = 2 unpaired e^-; U^{5+}, Np^{6+} = 1 unpaired e^-) and Fe^{2+} (4 unpaired e^-) were set in a ferromagnetic configuration with net alpha (upward) spin, and the net spin of the system is conserved in each calculation. Antiferromagnetic spin coupling was explored in a subset of inner-sphere calculations, but this spin configuration was not applied for entire reaction coordinate series due to the difficulty in getting correct initial spin assignment at large reactant distances. The atomic charges and spins in the system were determined using Mulliken population analysis. Mulliken results were compared with Bader [55, 56] and natural [57, 58] population analyses and the difference was ≤0.2 charge or spin units [41]. The use of a more rigorous population analysis approach did not change the interpretation of charge or spin change in the system. A small subset of models in this system were tested and verified to have similar variability between the different population analysis methods. From here on, discussion of atomic charge and spin refer to the results of Mulliken population analyses. All three carbonate groups of the $[AnO_2(CO_3)_3]^{5-/4-}$ complex are in a bidentate configuration and lay in the equatorial plane around the actinyl molecule as has been described by various experimental [11–13, 15–17, 59, 60] and computational studies [14–16, 61]. Our calculated structures for these complexes align, in terms of bond distances and angles, with these previously reported data. The C-PCM implicit polarizable conductor model, a robust and widely-applied implicit hydration scheme [32, 62–65], was used to simulate the contribution of higher-order solvation shells to the energy of the system [66, 67].

To evaluate the kinetics of reactions between a given actinyl and reductant complex, a series of geometry optimization calculations, in which the distance between the actinide and reductant (either the Fe or S atom) was held constant for a given configuration along the reaction path (while all other atoms were allowed to relax), were conducted at progressively shorter distances. Starting from a relatively large actinide-reductant distance (9–12 Å), the reductant is stepped towards the actinide in 0.25 Å increments, to a distance of ~2 Å. The geometry is optimized at each step and the atoms comprising the reductant and its first coordination shell are taken and shifted to generate the next input orientation. The (Kohn–Sham) orbitals from the previous geometry are supplied as a starting point for the initial electronic configuration. The incoming reductant was set to travel along the x axis of the system on a trajectory to impact the actinyl tricarbonate complex between two carbonate groups that are lying in the x-y plane. The actinyl molecule is positioned along the z axis, with the An center defining the origin of the coordinate system.

For the purpose of deriving kinetic parameters, the goal of these calculations is to generate an energy versus distance curve (see Figure 2 for an idealized schematic). At large reactant distances, the energy of the system is nearly a plateau with a very shallow slope. There is very little

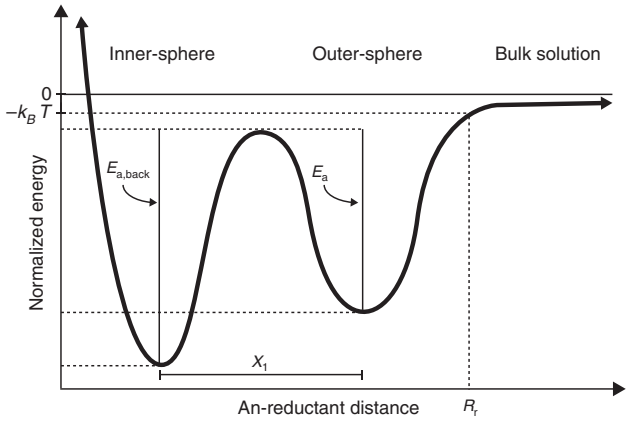


Figure 2: A schematic energy versus distance relationship showing the decrease in energy associated with bringing a reductant closer to an actinide (An) species in solution.
The position of the reactive radius (R_r) is indicated, as are the activation energies (E_a) for the forward and backward reactions and the distance between the two energy minima (x). These parameters are gathered from the calculated reaction distance series and used to evaluate the rates of transitions between different complex configurations.

interaction between the two complexes at these distances and the slope, however small, is due to long-range electrostatic forces. Testing of this distance regime has revealed that the slope directly correlates to Coulomb interaction energy and is very small when the distance is >10 Å and the atoms are screened by a solvent (e. g. water in explicit and/or implicit form via C-PCM) [41]. Eventually, there is a point at which this energy slope increases and the energy becomes more negative to a local minimum corresponding to the energy of an outer-sphere complex. This configuration is defined by hydrogen bonding between the intact coordination shells of the two reactants and the lack of direct bonding interaction between Fe or S with carbonate O or the actinyl (these latter features define the inner-sphere complex configurations). The point along this downward trajectory when one k_BT unit (2.49 kJ/mol vs. the energy of infinite separation between the actinyl and reductant) of energy has been gained is defined as the reactive radius (R_r). With this amount of energy gained, the system is far enough down the path toward the formation of the outer-sphere complex such that escape back to the solution bulk is unlikely.

The reactive radius is used in this study to determine the rate of encounter complex formation from the collisions of free coordination complexes in a bulk solution. The following equation, based on collision theory, is used to determine this initial collision rate (r):

$$r = \pi R_r^2 \nu N_A [X][Y] \tag{3}$$

where R_r is the reactive radius (in dm; dm is used here to correspond to the unit for volume of solution, which is L or dm^3), ν is the geometric mean of the diffusion velocities (each derived from a diffusion coefficient, D, by dividing by the ionic diameter and a geometric factor, approximately equal to 1 in solution) of the reactants (in dm/s), N_A is Avogadro's number, and [X] and [Y] represent the concentrations of the reactant species (in M). Diffusion coefficients for the reductants Fe^{2+} (7.19×10^{-8} dm^2/s) and H_2S (1.48×10^{-7} dm^2/s) are taken from the experimental literature [68, 69]. The diffusion coefficient of the actinyl tricarbonate complex (5.52×10^{-8} dm^2/s) is assumed to be constant across the different actinide elements and valence states [70]. This assumption is a fair one given that variability in the diffusion coefficients of different actinyl water and carbonate complexes is minor or not measureable [37, 71, 72]. If one reactant is considered to be much larger than the other, say the concentration of reductant [Y] is in great excess to the actinyl carbonate complex, [X], then nearly all of Equation 3 can be simplified into a pseudo-first order rate constant. Within the calculated reactive radii range found in this study, and assuming [Y] = 1 μM, this constant falls within 4502–6018 s^{-1}.

This collision rate is used to calculate the formation of outer-sphere complexes from bulk solution concentrations. Next, the rate(s) of transition from outer- to inner-sphere complex configurations, or between consecutive outer-sphere complex configurations, are determined. Both the forward and backward transitions between different complexes are considered. In some cases, the system energy versus distance relationships show smooth parabolic energy wells, but others appear less symmetrical and even appear like sloped steps. These aberrations from an idealized energy surface, as shown in Figure 2, are due to the complexities of hydrogen bonding networks and the "snap" formation of new bonds for which the energy response is dramatic due to the relatively low number of explicit solvent molecules included in the system [41]. The rate constants (k_r) for these transitions are calculated using the Arrhenius equation:

$$k_r = Ae^{\frac{-E_a}{RT}} \tag{4}$$

which depends on a pre-exponential factor, also called the attempt frequency (A), the activation energy of the process (E_a, in kJ/mol), the gas constant (R; not to be confused here with the reactive radius, R_r), and temperature (T; in this case, 298.15 K). The attempt frequency of the transition is itself a function of several factors and is also related to the activation energy, the mass (m, in kg) of the

Table 1: Calculated reactive radii (R_r, in Å) for different $[AnO_2(CO_3)_3]^{x-6}$-reductant[a] pairs.

Actinyl	Reductant	
	Fe^{2+}	H_2S
UO_2^+	8.5	9.3
UO_2^{2+}	9.2	9.5
NpO_2^+	8.6	9.5
NpO_2^{2+}	9.0	8.7
PuO_2^+	8.2	9.2
PuO_2^{2+}	8.9	8.7

[a]Unpaired spins on Fe^{2+} and actinyl, when present, are in a ferromagnetic arrangement.

incoming reductant complex ($Fe(OH)_2(H_2O)_4$ or $H_2S(H_2O)_6$), moving over the energy barrier and the distance between the two energy minima on either side of the activation energy peak (x, in m):

$$A = \frac{1}{\sqrt{2}}\sqrt{\frac{E_a}{mx^2}} \quad (5)$$

Equation 5 was originally applied to diffusion of atoms in crystal lattices [73, 74] and the difference between calculated attempt frequencies and those derived from fitting a parabolic function was found to be minimal [41]. As such, this simpler approach, for which all the necessary inputs can be extracted readily without any curve fitting, is applied again here.

For every reactive pair, a minimum of three different rates are considered: (1) the rate of encounter complex formation from collision theory using Equation 3, (2) the rate of the transition from outer- to inner-sphere complex using Equations 4 and 5; and (3) the rate of the back reaction where inner-sphere complexes return to the outer-sphere complex configuration. For systems with more than one energy barrier, more forward and backward reactions are added to the model. These different rates are used as inputs to a computer program that evaluates the change in concentration of different complex species starting from concentrations of the free reactants, the actinyl tricarbonate and reductant-water complexes, in the simulated solution. These aqueous reactants are consumed via the collision reaction and are then subject to the outer- and inner-sphere complex transition rates. The concentrations of all the different species (e. g. [H_2S in bulk solution], [outer-sphere complex], [inner-sphere complex]) are evaluated over small time increments to learn about the overall kinetics of the outer- and inner-sphere complex formation.

For further information regarding this approach for deriving aqueous redox reaction kinetics, the reader is referred to its first implementation in a prior study [41] focused on the reactions of PuO_2^+ and PuO_2^{2+} hydrolysis complexes, $[PuO_2OH(H_2O)_4]^0$ and $[PuO_2(OH)_2(H_2O)_3]^0$, with Fe^{2+}, Fe^{3+}, and hydroxyl radical, where the methodology is described and evaluated in more detail. A subset of the structures in this study were recalculated using different computational parameters to see how the inclusion of a dispersion term might affect the energetics and kinetics. The dispersion calculations (DFT-D) were carried out using the same B3LYP functional, basis set, pseudopotential, but include Grimme's D3 dispersion model with Becke–Johnson damping (GD3BJ) [75, 76]. For this same subset of structures, replicate calculations were also calculated without dispersion to determine the thermodynamic parameters of enthalpy, entropy, and Gibbs free energy (G) and assess the difference between Gaussian electronic energy, referred to in this paper as E, and G.

3 Results

This section starts with the calculation of the collision frequency of the actinyl tricarbonate complex with a reductant. For this calculation, the reactive radius (i. e. the distance at which reactants interact more strongly than their thermal motion) in solution is a governing variable. This step, which is followed by outer- and inner-sphere complex formation, is calculated using a combination of statistical mechanics and quantum mechanics.

3.1 Calculated reactive radii

The reactive radius (R_r) for all of the different reactant pair combinations was determined by making a linear fit between the two distance steps bracketing the energy gain of one k_BT unit from the bulk solution energy plateau and assumes the molecular interaction overcomes the thermal motion of the reacting particles. The calculated distances are presented in Table 1 and fall within 8.2–9.5 Å. The distances for reactions with $Fe(OH)_2(H_2O)_4$ are generally smaller than those for $H_2S(H_2O)_6$. The two exceptions are the reaction of the PuO_2^{2+} and NpO_2^{2+} tricarbonate complexes with Fe^{2+}, which have reactive radii that are 0.2 and 0.3 Å larger than their H_2S counterparts, respectively. The shorter radii observed for most of the Fe^{2+} reactions may be explained by the coordination of iron by the two hydroxide ions. It is possible that the interaction between OH^- and Fe^{2+} masks some of the long-range electrostatic interaction and that there may even be a slight repulsive component between OH^- and the CO_3^{2-} groups. In addition, the

charged Fe cation more tightly binds the members of its first coordination shell relative to H_2S. As a result, the H_2O molecules that were initially placed in octahedral coordination around the H_2S are more likely to drift out of position. The formation of H bond chains connecting several waters stretching into the gap separating the actinyl carbonate and reductant coordination complexes effectively shortens the reactive radius. These water chain structures were found to form for nearly all of the H_2S reactions, but did not form as coherently in the reactions with divalent neptunyl and plutonyl, explaining the relatively short reactive radii compared to the others.

These reactive radii, along with the diffusion coefficients of the reactant species, are used to calculate the rate of encounter complex formation (see Equation 3). This aqueous encounter rate increases with increasing concentrations and diffusion velocities. The more molecules or complexes that are present and the faster they are traveling, the more likely they are to pass within R_r of each other and form an energetically-favorable outer-sphere complex.

3.2 Rates of outer-sphere complex formation

Once the reactive radius is reached, energy surfaces for all of the tested reactions paths show an increase in slope, representing the energy gain associated with the start of outer-sphere complex formation. The rate of collision and formation of the outer-sphere complexes was assessed using the computer script described above in the Section 2. Initial collision rates were calculated and then reevaluated over small time increments. These subsequent rates take into account the decrease in concentration of free aqueous reactants over time as outer-sphere (and inner-sphere) complexes are formed. One way to frame the rate at which this process occurs is to consider a half-life ($t_{1/2}$, the time at which half the free aqueous complex has been converted to an OSC or ISC) of the free actinyl tricarbonate complex which has not yet formed an outer-sphere complex via collision with a reactant in solution. The concentration of the free actinyl carbonate complex decreases rapidly and effectively goes to zero if the concentration of the second reactant (in this case, the Fe^{2+} and H_2S water +/− hydroxide complexes) is in significantly higher concentration. The half-lives for several of the reaction pairs, with different initial reactant concentrations, are presented in Table 2. Larger reactive radii, faster diffusion, and higher concentration all decrease $t_{1/2}$. Even at environmentally-relevant actinyl concentrations, typically in the nM to pM range, outer-sphere complex formation is calculated to proceed rapidly with significant complex formation occurring over several ms to s. Half of the available free actinyl tricarbonate complexes will form outer-sphere complexes with reductant species within 11.5–15.4 s with starting concentrations of 1 pM and 1 nM, respectively. These half-lives decrease to ms. and μs. if concentrations are increased to the μM and mM level.

Energy minima associated with outer-sphere complex formation are noticeably different for reactions with Fe^{2+} and H_2S. In the case of reactions with Fe^{2+}, the outer-sphere positions are defined by smooth-sided energy wells with local minima at An–Fe = 6 Å. This distance is almost the same nearly independent of type of actinide or oxidation state. For the reactions with H_2S, the energy surfaces are less uniform across the different actinyls. Energy minima positions for the outer-sphere complexes with H_2S range between An–S distances of 4.3–5.5 Å. Of the six tested H_2S reactions, the outer-sphere complex with UO_2^+ tricarbonate has the largest An–S distance at 5.5 Å. No other outer-sphere complex has an An-reductant separation larger than 5 Å. The energy wells with H_2S are also steeper-sided than those of Fe^{2+} and show particularly rapid energy increases as the An–S distance is decreased. After the reactive radius, energy versus distance curves of H_2S show relatively shallow slopes leading up to the edges of these steep-sided outer-sphere energy wells, whereas the Fe^{2+} curves show a steeper, but smoother, trajectory down into the local minimum. The energy curves of all of the different tested reaction pairs are presented in Figure 3.

The structures of these different outer-sphere configurations reveal that beginnings of the energy wells correspond to the formation of multiple H bonds between the coordinating water molecules around Fe^{2+} and H_2S and the O atoms of actinyl-coordinating carbonate groups. In the

Table 2: Calculated half-lives ($t_{1/2}$) of free actinyl tricarbonate complexes in solutions with the reductants Fe^{2+} and H_2S at different reactant concentrations.

[Actinyl]	[Reductant]	UO_2^{2+}/Fe^{2+}	UO_2^+/H_2S	NpO_2^+/H_2S	PuO_2^+/Fe^{2+}
1 μM	1 mM	12.2 μs	14.4 μs	11.5 μs	15.4 μs
1 nM	1 μM	12.2 ms	14.4 ms	11.5 ms	15.4 ms
1 pM	1 nM	12.2 s	14.4 s	11.5 s	15.4 s

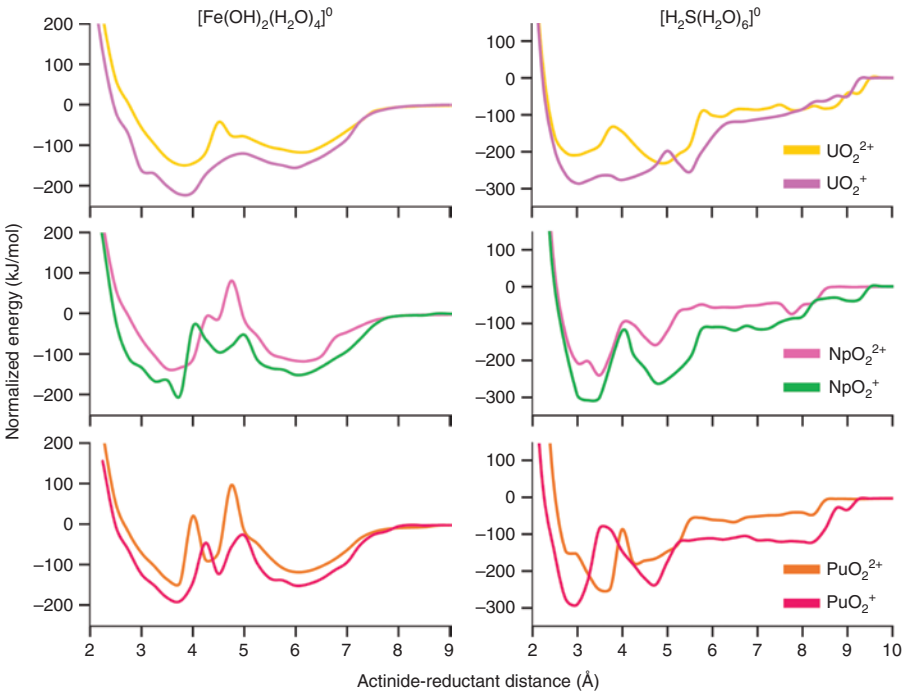


Figure 3: Calculated energy versus distance curves for actinyl tricarbonate, $[AnO_2(CO_3)_3]^{x-6}$, complexes reacted with $[Fe(OH)_2(H_2O)_4]^0$ and $[H_2S(H_2O)_6]^0$. Energies (in kJ/mol) are normalized so that zero represents the energy of the reactants in the bulk solution (An-reductant distances >9 Å). Outer- and inner-sphere energy minima are defined in the regions of 4.25–6 Å and 3–3.75 Å, respectively, and vary between different actinyls and valences.

calculations, H_2S has a less ordered coordination environment and as such, the formation of these bonds between carbonate and water is more varied. Once a H bonding network is established, the water in these models quickly seeks to arrange itself which results in steeper-sided energy wells. In the case of Fe^{2+}, the water and hydroxide are more ordered around the cation and the changes to these water molecules are more gradual as they balance the energy gains associated with coordinating the cation versus forming a H bond to carbonate.

In the case of H_2S, the formation of the outer-sphere complex is coincident with the loss of a proton and conversion to HS^-. This behavior is observed in all H_2S series that were tested. This proton is passed first to an adjacent water molecule, which in turn gives up one of its own protons to a carbonate group to create bicarbonate (HCO_3^-). The bicarbonate initially remains in bidentate configuration around the actinyl, but eventually, as the An–S distance decreases, becomes monodentate. An example of this structure immediately following H^+ transfer, for the reaction with UO_2^{2+}, is presented in Figure 4. This change is also accompanied by spreading and bending of the two (bi)carbonate groups out of the plane due to electrostatic repulsion between negatively-charged S and O of carbonate. In comparison, incoming $[Fe(OH)_2(H_2O)_4]^0$ causes only minor changes to carbonate coordination of the actinyls. The $An–O_{carbonate}$ and An–C distances lengthen slightly, on the order of 0.1–0.2 Å, as H bonds form to water. The

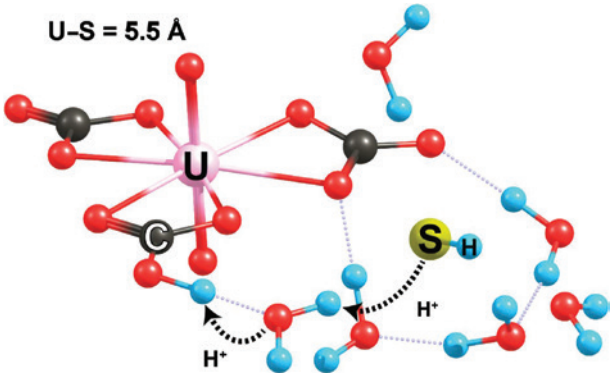


Figure 4: The structure of an outer-sphere complex of H_2S with $[UO_2(CO_3)_3]^{4-}$ at a U–S distance of 5.5 Å.
At this distance, H_2S has passed a proton via a neighboring water molecule to CO_3^{2-} to form HCO_3^- and HS^-. The bicarbonate molecule remains in bidentate configuration at this distance, but as the HS^- is brought closer to U, both the bicarbonate and adjacent carbonate will begin to bend out of the equatorial plane and rotate to become monodentate around the central actinyl. This motion will result in an energy barrier between outer- and inner-sphere energy minima. Similar structures are observed for the other actinyl complexes in reactions with H_2S.

carbonate molecules rotate like a wheel as Fe^{2+} is brought closer such that the inner carbonate O atoms are pushed in towards the An center. As such, each $An–O_{carbonate}$ distance on the two carbonates closest to the Fe changes by about the same amount, but some increase and some decrease. No proton transfer from water to carbonate is observed in the Fe reaction series. A representative outer-sphere complex configuration is presented for the reaction of $[Fe(OH)_2(H_2O)_4]^0$ with $[PuO_2(CO_3)_3]^{5-}$ in Figure 5a. In this configuration, a water molecule has oriented itself flat in the x-y plane to form H bonds with two carbonate groups; this geometry corresponds to the outer-sphere energy minimum in this reaction.

3.3 Formation of inner-sphere complexes and associated energy barriers

In all tested reactions, there is an energy barrier associated with the transition from an outer- to inner-sphere complex. This energy barrier is observed in the An-reductant distance range of 3.5–5 Å. In several reactions with Fe^{2+}, two energy barriers are present that separate multiple outer-sphere complex configurations from the inner-sphere complex. The barriers for the reactions with Fe^{2+} fall in a narrower An-reductant range (4–5 Å) than for H_2S. The activation energies range widely between 11 and 215 kJ/mol across the different reactant pairs. A full

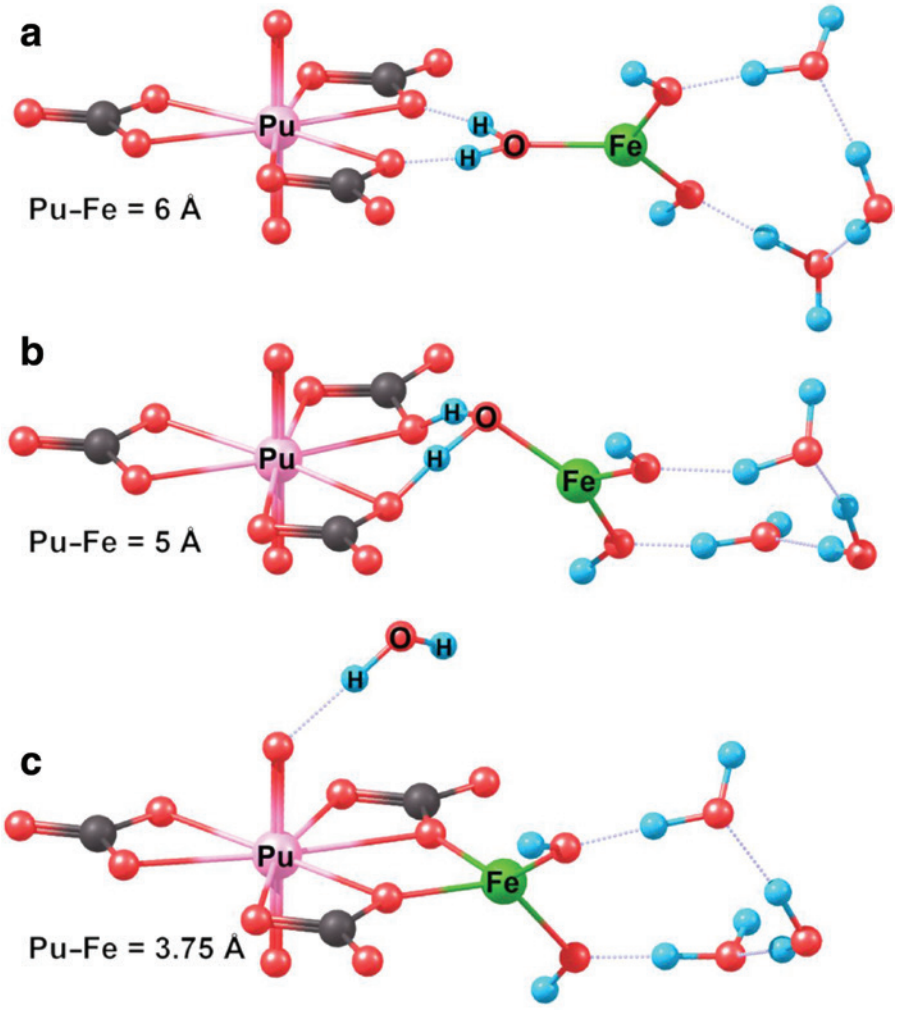


Figure 5: Geometries of outer-sphere, transition state, and inner-sphere complexes for the reaction of plutonyl tricarbonate with ferrous iron. Panels a, b, and c show the approach of an $[Fe(OH)_2(H_2O)_4]^0$ cluster towards $[PuO_2(CO_3)_3]^{5-}$ at Pu–Fe distances of 6, 4, and 3.75 Å, respectively. These distances correspond to an outer-sphere complex (a), and inner-sphere complex (c), and a transition state between them (b). A water molecule forms a hydrogen bond to two carbonate groups in panel c, but in the transition to the inner-sphere complex, this molecule is squeezed up out of the x-y plane which holds the carbonate groups, Pu, and Fe. In panel c, this molecule is now hydrogen bonded to one of the plutonyl O atoms. The energy cost associated with breaking the water hydrogen bonds the main source of the E_a between the outer- and inner-sphere complex.

Table 3: Calculated activation barrier parameters for reactions of actinyl tricarbonate complexes with $[Fe(OH)_2(H_2O)_4]^0$ and $[H_2S(H_2O)_6]^0$ using the C-PCM solvation model.

Reductant	Actinyl	Activation energies (E_a, in kJ/mol) and distances between energy minima (x, in Å)		
		E_a	$E_{a,back}$	x
Fe^{2+}	UO_2^+	$E_{a1} = 35$	101	2.25
	UO_2^{2+}	$E_{a1} = 74$	106	2.25
	NpO_2^+	$E_{a1} = 99$	43	1.5
		$E_{a2} = 65$	171	0.75
		$E_{a3} = 37$	2	0.5
	NpO_2^{2+}	$E_{a1} = 199$	217	2.5
	PuO_2^+	$E_{a1} = 125$	96	1.5
		$E_{a2} = 77$	145	0.75
	PuO_2^{2+}	$E_{a1} = 215$	185	1.75
		$E_{a2} = 35$	165	0.5
H_2S	UO_2^+	$E_{a1} = 57$	79	1.5
		$E_{a2} = 11$	21	1
	UO_2^{2+}	$E_{a1} = 12$	137	1.25
		$E_{a2} = 96$	75	2
	NpO_2^+	$E_{a1} = 142$	188	1.5
	NpO_2^{2+}	$E_{a1} = 59$	142	1.25
	PuO_2^+	$E_{a1} = 152$	208	1.75
	PuO_2^{2+}	$E_{a1} = 89$	164	0.75

list of the calculated activation energies for the forward and backward reactions over these barriers, as well as the distance between energy minima for the different reactant pairs, is presented in Table 3. The large spread in energies is related to the variety of different structural changes that happen as the reductant is brought closer to the actinyl tricarbonate complex and the behavior of the explicit water molecules. Hydrogen bonds between water and carbonate, and in the case of H_2S, proton transfer to form HCO_3^- and HS^-, define the outer-sphere complex regime. As Fe^{2+} and HS^- move closer to the carbonate groups, these systems undergo different styles of structural reorganization.

For both reductants, water and/or hydroxide molecules that comprise the explicitly-modeled first coordination shells are forced to rearrange themselves. The one or two molecules that are between the incoming reductant and the carbonate ring are most affected by the shrinking An-reductant distance. Several optimized structures are shown in Figure 5 as $[Fe(OH)_2(H_2O)_4]^0$ is brought closer to $[PuO_2(CO_3)_3]^{5-}$. The H bonds of one water molecule to two carbonate groups are shown in the first panel, corresponding to a Pu–Fe distance of 6 Å. The second structure, in panel B, shows the system at a distance of 5 Å at the crest of an energy barrier to form a second outer-sphere configuration. In the third step, the water molecule has no interaction with the carbonate at all and is now H bonded with one of the actinyl O atoms. This position of H_2O in an H bonding configuration with actinyl O is observed for approximately half of the reaction pairs. There does not seem to be an obvious reason why some systems adopt this configuration in the inner-sphere complex when others do not. In the cases where it does occur, it always corresponds to the minimum energy configuration for the reaction distance series. However, similar energy gains over the outer-sphere complex energy are still achieved in systems where H bonding to actinyl does not occur.

In the case of the reaction shown in Figure 5, the energy barrier between panels A and B is quite large (125 kJ/mol). As such, the concentration of the inner-sphere complex remains negligible over time if the tested pathway of structural change is assumed. This reaction, along with others, were tested over time periods of up to 15 s and for reactions with E_a values larger than ~100 kJ/mol, the transitions are prohibitively slow at standard temperature conditions. This varies somewhat with the distance between the energy minima (x), which affects the attempt frequency as shown in Equation 5, but this cutoff value encompasses the majority of the data. The change in concentration of the different complex configurations (bulk solution, outer-sphere and inner-sphere) is shown in Figure 6 for the reactions of monovalent and divalent uranyl tricarbonate and their reactions with incoming Fe^{2+}. The calculated concentration changes show that for UO_2^+ (Figure 6a), the outer-sphere complex is rapidly consumed due to the relatively low energy barrier for inner-sphere complex formation. In the case of UO_2^{2+} (Figure 6b), the kinetic barriers are such that the outer-sphere complex is more slowly converted into the inner-sphere complex configuration over time.

Large activation energy barriers also exist in reactions with incoming H_2S. In these reactions, the molecules initially move in a similar fashion to the Fe^{2+} calculations, but after a proton is transferred from H_2S to form bicarbonate, the (bi)carbonate groups begin to experience significant electrostatic repulsion. As HS^- gets closer to the actinyl, water molecules move out of the x-y plane as the Fe-coordinating waters did in Figure 5. However, within An–S distances of ~4.75 Å, the (bi)carbonate groups begin to bend and rotate out of this plane to position their O atoms further from HS^-. There is a significant energy cost associated with this disruption of the actinyl coordination environment. These changes to the geometry, along with breaking and forming of different hydrogen bonds between water and (bi)carbonate, are the source of the energy barriers in these reactions. The carbonate groups around the actinyl molecules can show extreme disruption from their

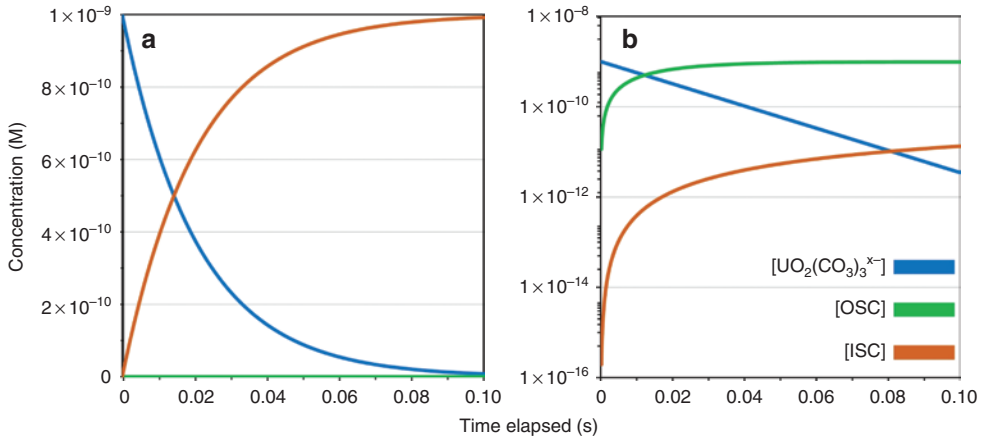


Figure 6: Calculated change in product and reactant concentrations over time for uranyl tricarbonate reacting with ferrous iron. Panels a and b show the change in concentration of bulk aqueous uranyl tricarbonate along with inner- and outer-sphere complexes (OSC and ISC) with $[Fe(OH)_2(H_2O)_4]^0$ over time starting from initial bulk uranyl and iron complex concentrations of 1 nM and 1 μM, respectively. The reaction with UO_2^+ in panel a has a small energy barrier for the formation of the ISC and, as such, the aqueous complex is rapidly converted to the ISC with no appreciable pool of OSC forming over time. The reaction of UO_2^{2+} on the other hand has an activation energy large enough to allow for relatively rapid build up of the OSC followed by a slower increase in the concentration of the ISC. The concentrations in panel b are shown on a log scale to better capture the large concentration range.

initial equatorial configuration, tilting by up to ~70 ° out of the x-y plane when HS^- is brought to its closest distances. In all of these inner-sphere configurations, the two (bi)carbonate groups that have been split by the incoming bisulfide switch to monodentate coordination of the actinyl and the overall coordination of the actinide drops from 6 to 5. Surprisingly, the energies of these inner-sphere complex geometries, where An is directly coordinated by S are energetically favorable compared to the outer-sphere complexes. However, some, like the reactions with NpO_2^+ and PuO_2^+, are kinetically prohibited given the large activation barriers (see Table 3).

In nearly all reactions, the inner-sphere configuration represents the minimum for the system (see Figure 3). The one exception is the reaction of UO_2^{2+} tricarbonate with H_2S, which has an outer-sphere complex that is 20 kJ/mol more favorable than the inner-sphere configuration. This is due to bending of (bi)carbonate out of the plane and a relatively unfavorable H bonding network, specifically, with no H bonds formed to the actinyl O as is observed in other H_2S reactions. The energy gains associated with inner-sphere complex formation come from changes to the physical structure (i. e. hydrogen bonding and An coordination) and are not due to significant changes in the electronic structure of the system (i. e. electron transfer from Fe^{2+} or HS^- to the $An^{5+/6+}$). In every one of the tested reaction paths, population analysis of the atomic charge and spin reveals that the oxidation states of the actinides, and reductants, are preserved throughout the reactions. The ferromagnetic spin configuration, which orients all of the unpaired electrons in the same direction (upward spin), could allow transfer of minority spin electrons (downward spin) electrons to result in an antiferromagnetic configuration; however, this is not observed. This result suggests that the reduction of An^{6+} to An^{5+} by Fe^{2+} or H_2S may not be spontaneous even if the kinetic barriers to inner-sphere complex formation have been overcome.

3.4 Effect of dispersion terms and frequency analysis on reaction kinetics

For the uranyl tricarbonate and Fe^{2+} reaction, additional calculations were performed to assess the impact of dispersion on the overall system. The inclusion of a dispersion model was considered as it has the potential to improve the accuracy of weak bonding interactions, such as H bonds, that play a significant role in the complex formation and outer- to inner-sphere transition. Structures calculated at the B3LYP level of theory were used as a starting point for DFT-D calculations with the GD3BJ dispersion model. Seven points along the reaction path were selected to be recalculated and the energy difference between these new values and the original *E* was determined (see Figure 7b). These points were fit with polynomial functions to allow a reactant distance-dependent shift to be determined and applied to the rest of the distance points. A similar approach was used to assess the Gibbs free energy of these complex formation reactions. Frequency calculations were carried out on the same seven distance points using the original computational parameters (B3LYP, etc.). From this vibrational analysis,

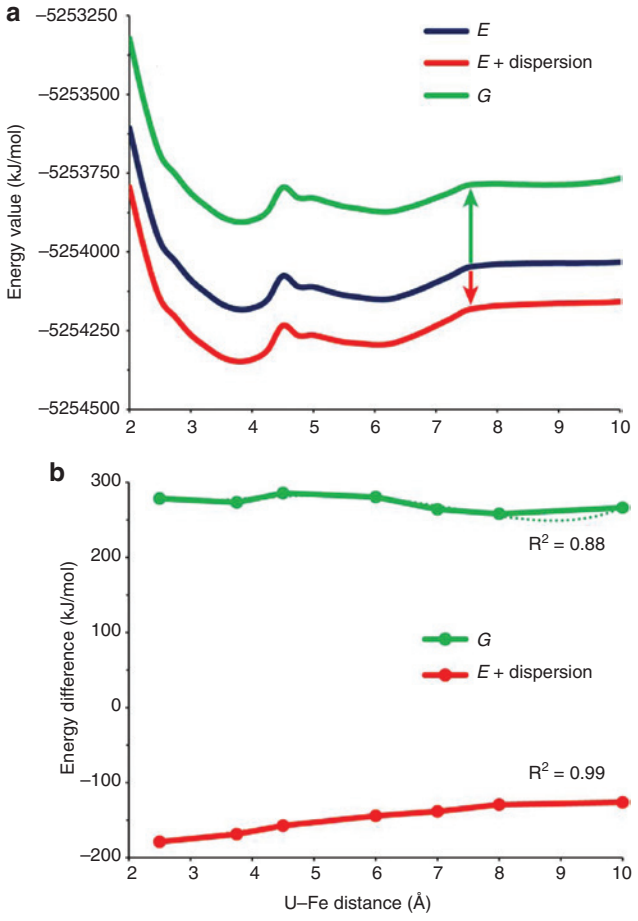


Figure 7: Impact of DFT-D and frequency analysis on reaction kinetics. Panel a presents the energy (in kJ/mol) versus distance relationships for $[UO_2(CO_3)_3]^{4-}$ complex reacting with Fe^{2+}. The three curves show the original B3LYP electronic energy (*E*, in blue), DFT-D energy curve with GD3BJ dispersion model (in red), and the Gibbs free energy (*G*, in green), as determined via frequency calculations. Panel b shows the energy difference between the original *E* and the values calculated with new parameters at selected distance points. These seven points were then fit with polynomial functions (the dotted lines; R^2 values shown) to yield the distance-dependent energy shift that was then applied to the rest of the distance range to generate the curves in panel a.

the enthalpy and entropy of the system were determined and used to calculate the *G* at 298.15 K.

Both changes to the original computational parameters result in a gain or loss in energy (shift of the energy curves in Figure 7a downward and upward). Inclusion of dispersion results in an energy gain associated with the H bonding networks between the explicit solvent molecules in the models. In the case of *G*, there is a loss of energy associated with the change from a purely electronic energy (*E*) to one that includes zero-point vibrational modes and the entropic term. Despite the overall shift the energy curves, the shape and position of features along the reaction pathway are relatively unaffected. In the reaction presented in Figure 7, the positions of the outer- and inner-sphere energy wells remain the same. The activation energy barrier for the forward reaction decreases by 7 % in the DFT-D case and increases by 3 % when using the Gibbs free energy. Overall, these differences are <10 kJ/mol and if combined into a net factor represent a change from the B3LYP electronic energy-derived E_a of only −4 %. From these results, it appears that the electronic energy, without the use of more expensive frequency calculations to determine the ΔG, are sufficient for describing the kinetics of these systems within a reasonable margin of error (<5 %).

3.5 Testing of proton-coupled electron transfer as a mechanism for actinyl reduction

Prior work on plutonyl pentaquo complexes [41] and another computational study of uranyl tricarbonate [38] have found that proton-coupled electron transfer (PCET) may be a critical step in the reduction of actinyl species. Since no spontaneous proton transfer (PT) to actinyl O was observed in the reaction paths described above, some further investigation of post-PT structures, where the proton was moved manually, was carried out to see if this would trigger electron transfer (ET). This subset of calculations used a representative inner-sphere complex geometry of uranyl and plutonyl tricarbonate with Fe^{2+} (An–Fe = 3.75 Å) as a starting point. This geometry was selected because it represents the minimum energy distance from our calculations and rates of inner-sphere ET are known to be faster versus the outer-sphere for Fe^{2+} reactions with uranyl species [31, 38, 77]. The system was made charge-neutral by adding four protons to the $[AnO_2(CO_3)_3]^{4-}$ – $[Fe(OH)_2(H_2O)_4]^0$ system. These protons were placed on the two hydroxide groups (to form two additional explicit water molecules) and the two carbonate groups closest to Fe to create two HCO_3^-. Different post-PT geometries were then tested to see what PT mechanism was most energetically favorable and to explore if these changes to the geometry are accompanied by reduction of the actinyl. Proton transfer from bicarbonate and water was tested and protonation of a single and both actinyl O was explored. Additionally, ferromagnetic and antiferromagnetic (where Fe is spin up and the An is spin down) spin configurations were tested to see if this had an impact on the energetics of the reaction and behavior of the Gaussian code in assigning spins in the system.

We determine that for uranyl, PT with or without ET is a very selective process, with only one of the tested

pathways yielding exothermic PCET. This reaction corresponds to a ferromagnetic system where the spin multiplicity of the pre-ET and post-ET models is not the same (multiplicity increase from 5 to 7 for the post-ET state with U^{5+} and Fe^{3+}) and a single proton is transferred from bicarbonate. The reaction energy (ΔE) of this process is –2.5 kJ/mol. Several other PT pathways also resulted in reduction of U^{6+} to U^{5+}, but they are all endothermic with ΔE values ranging between 20 and 207 kJ/mol. For the uranyl complexes, reaction energies are lower when H^+ is transferred from bicarbonate ($\Delta E = -2.5$–25 kJ/mol) versus water ($\Delta E = 56$–207 kJ/mol). The most unfavorable reactions correspond to the transfer of two H^+ each from a different water molecule to protonate both actinyl O atoms. In reactions that do show reduction, the net spin on U changes from 0 to 1.1 as expected for a transition from U^{6+} with no unpaired electron to U^{5+} with one; the Fe spin increases from ~3.7 (≡Fe^{2+} with 4 upward spins) to ~4.4 (≡Fe^{3+} with 5 upward spins). Representative pre- and post-PCET structures with projected spin densities on U and Fe are presented in Figure 8. Aside from the one exothermic reaction, the other pathways that record ET have higher reaction energies ($\Delta E = 20$–207 kJ/mol) compared to PT reactions without ET ($\Delta E = 8$–16 kJ/mol). An example is the transfer of a single proton from HCO_3^- with an antiferromagnetic spin configuration (i. e. no change in multiplicity of the system pre- and post-ET). This reaction did not cause ET, but had a relatively low reaction energy of 16 kJ/mol. Proton transfer from a water molecule to create OH^-, similar to the PCET reaction observed in prior calculations of plutonyl hydrolysis complexes [41], results in reduction of U^{6+} by Fe^{2+}, but has an endothermic reaction energy of 57 kJ/mol. In order to test how much of an electric field gradient would be required to "help" in the electron transfer process, a small subset of these UO_2^{2+} inner-sphere complex structures were tested with an applied electric field. This field was approximately parallel to the line connecting Fe and U (the x axis of our system) and was set to pull electron density from the Fe^{2+} to the actinyl to see if ET was possible without PT. It was found that while eventually the system did reduce U^{6+} to U^{5+}, the electric field strength required (0.0125 atomic units) is relatively high and reflects the ability of carbonate to effectively shield actinyl molecules from reductants. The results described here are included in further detail in Table S1 of the Supplementary Information.

For the PuO_2^{2+} tricarbonate complex, the same pre- and post-PT configurations were tested. The PCET reactions are more likely to be energetically-favorable and reduction of Pu^{6+} to Pu^{5+} occurred in nearly all cases where one or two protons are transferred. Reaction energies for the tested PCET reactions range between –5 and 172 kJ/mol (spin on Pu increasing from ~2.5 to ~3.6 indicating reduction to Pu^{5+}). The only reaction that does not yield ET is the transfer of one H^+ from HCO_3^- with a ferromagnetic spin arrangement ($\Delta E = 120$ kJ/mol). Two of the tested PT mechanisms resulted in negative reaction energies: transfer of one H^+ from a water molecule and transfer of two H^+ from two bicarbonates. Both of these reactions have antiferromagnetic spin configurations where multiplicity is conserved after ET (Fe spin up and Pu spin down) and have comparable reaction energies of –5 kJ/mol. The spread in reaction energies is similar to that of uranyl, but with far more PT reaction pathways resulting in ET (ΔE values between –5 and 171 kJ/mol). Broadly, the reaction energies of PT and PCET for plutonyl are lower than those of equivalent uranyl reactions. Table S2 in the Supplementary Information further details the results of these plutonyl proton transfer calculations.

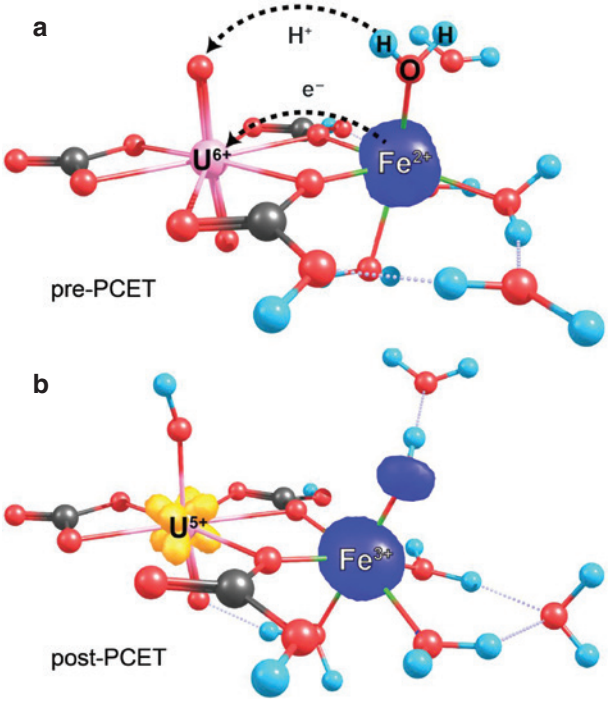


Figure 8: Representative pre- and post-proton coupled electron transfer complexes.
Structures of a charge-neutral $[FeUO_2CO_3(HCO_3)_2(H_2O)_6]^0$ inner-sphere complex before (a) and after (b) a proton-coupled electron transfer (PCET) reaction. This particular reaction has a $\Delta E = 56$ kJ/mol. Alpha (blue) and beta (yellow) spin density are shown overlain on the structure and clearly describe the transition from a U^{6+}/Fe^{2+} to U^{5+}/Fe^{3+} electronic state. The overall spin multiplicity of the system is preserved as U^{5+} takes on beta (downward) spin orientation. The H^+ is transferred from a water molecule to the uranyl O at the top of the structure and causes the $U–O_{ax}$ bond to lengthen from 1.8 to 2.0 Å. The remaining U–O double bond also lengthens, to 1.87 Å, with reduction to U^{5+}.

4 Discussion

The calculations in this study build upon a methodology that was initially applied to the reactions of Fe^{2+}, Fe^{3+}, and hydroxyl radical with monovalent and divalent plutonyl hydrolysis complexes without carbonate ligands [41]. The results presented here are the first fully quantum-mechanical treatment of actinyl tricarbonate reactions with Fe^{2+} and H_2S using a mixture of discrete water molecules and a dielectric continuum model to treat solvation. The calculations evaluate changes to the complex structures and the associated energy barriers over the selected reaction path. A number of phenomena captured in these calculations are in agreement with prior work on plutonyl [41]. For example, the energy gains and losses associated with changing the H bonding networks of colliding complexes are one of the major factors in the overall energetics of the reaction process. Indeed, in the reactions with Fe^{2+}, the energy changes are fully due to the arrangement of the H_2O and OH^- in the system and changes to the H bonding networks between them and eventually to the carbonate and/or actinyl O atoms. In the reactions with H_2S, the systems respond somewhat different as the reductant molecule eventually deprotonates to form HS^- and HCO_3^-. The energy barriers present in these reactions, while of similar magnitudes to the reactions with Fe^{2+}, are partly related to the significant disturbance of the (bi) carbonate molecules from their initial orientation caused by the approach of the negatively-charged species, HS^-. The rotation of these carbonates and their bending out of the equatorial plane impose significant energy penalties on the system that are only partially recovered by the formation of new H bonds and the eventual coordination of $An^{5+/6+}$ directly by HS^- in the inner-sphere complex geometries (An–S = 3–3.5 Å).

The activation energy barriers calculated for the tricarbonate complexes are larger than those for plutonyl hydrolysis complexes, which have a maximum E_a value for the forward reaction of 46 kJ/mol when using the C-PCM solvation model [41]. The coordination environments of the hydrolysis complexes, which consist of OH^- and H_2O, are apparently much more easily reorganized during the collision of an incoming reactant to form an inner-sphere complex. Coordination by carbonate, particularly three carbonate molecules which form a complete ring around the actinide center, represent a much more rigid complex geometry that is much harder to disrupt relative to a water and/or hydroxide complex. As such, the calculated activation energies for these complexes are significantly higher (see Table 3). It is reasonable to infer that actinyl complexes with a one or two carbonate molecules might have faster kinetics for inner-sphere complex formation with various reductants.

In this study, spontaneous reduction of actinyls by the two tested reductants is not observed. Population analysis of atomic charge and spin, as well as $An–O_{ax}$ bond lengths, do not indicate electron transfer from Fe^{2+} or H_2S/HS^- to either An^{6+} or An^{5+}. In our prior study of plutonyl hydrolysis complexes, reduction of Pu^{6+} to Pu^{5+} by Fe^{2+} is coincident with the formation of the inner-sphere complex and PT from coordinating water to one of the actinyl O atoms [41]. In another computational study [38], the redox reactions of a ternary complex of UO_2^{2+} tricarbonate with two Fe^{2+} were explored using a combination of atomistic molecular dynamics and quantum-mechanical calculations. The structure of this complex, with the formula $[Fe_2UO_2(CO_3)_3(H_2O)_8]^0$, is analogous to other actinyl tricarbonate complexes with two counter ions [10, 21, 22]. Each Fe^{2+} in this structure is coordinated by two carbonate groups and four water molecules. The positioning of the Fe^{2+} in this configuration is the most energetically-favorable configuration in Wander et al. [38] and is the same as the Fe position chosen for the collision trajectory in our models (see Figure 5c for an example). A PCET mechanism wherein a proton from water is transferred to create bicarbonate is thermodynamically- and kinetically-favorable for the reduction of U^{6+} to U^{5+} via a sequential reaction pathway (where ET and PT are considered as separate steps) [38]. Further reduction to U^{4+} by the second Fe^{2+} required significant structural reorganization and resulted in unfavorable reaction thermodynamics and kinetics.

With more time and computational power, the most rigorous treatment of these systems would be accomplished via a quantum-mechanical molecular dynamics (MD) simulations using a large number of explicit solvent molecules in addition to a dielectric continuum surrounding them. An approach like this, such as Car–Parrinello MD (CPMD) [78], would able to capture the dynamic process of H^+ transfer and a large number of solvent molecules would present multiple pathways for shuttling the proton and/or electron through the system. However, since the H bond breaking and forming happens so rapidly, it may not be trivial using a dynamic approach to reveal the transition state, and thus, the activation energy. Additionally, quantum-mechanical MD calculations of this sort are very computationally expensive and not particularly feasible when seeking to investigate a wide range of reactant pairs. Another possible change to the computational parameters would be to calculate the spin-orbit coupling of these reactant systems. Spin-orbit coupling influences the chemistry of species with unpaired spins such as Fe, U, Np, and Pu. Our treatment in this study uses a scalar relativistic

approach that neglects explicit treatment of the spin-orbit coupling energy that has the potential to affect some of the reaction energies in this study. However, since there is no observed change in the spin configuration over the course of our reaction paths (i. e. no electron transfer), the approach taken here is likely sufficient to describe, at the very least, the relative energetics of the different tested reactions.

In the calculations performed in this study, we opt for static quantum-mechanical calculations with a modest number of explicit solvent molecules for the first coordination shell and representing the rest of the solvation with the C-PCM model. This approach allows explicit water to move about during geometry optimization (including positions where they may serve as H^+ donors) and for the solvation energies to be, at least partially, recovered by the dielectric continuum model. Spontaneous transfer of protons is observed in the calculations with H_2S to form bicarbonate. In prior work on plutonyl hydrolysis complexes [41] using the same computational scheme, PCET from Fe^{2+} to reduce Pu^{6+} is observed with H^+ donation from H_2O to a plutonyl O. In the current study, spontaneous PCET from H_2S/HS^- and Fe^{2+} is not observed over any of the tested distance series. Instead, manual placement of a proton, from either bicarbonate or water, on an actinyl O is required to induce electron transfer from Fe^{2+}. In the tested cases for the uranyl and plutonyl complexes, the systems are selective for specific PCET pathways: the transfer of H^+ from HCO_3^- to actinyl O in the case of uranyl and transfer of H^+ from H_2O for plutonyl. These pathways represent a minority of the tested configurations; the other mechanisms are endothermic and/or did not yield electron transfer. In comparison, the study by Wander et al. [38] finds energetically- and kinetically-favorable PCET from Fe^{2+} to reduce UO_2^{2+} in a ternary complex with three carbonates and a second Fe^{2+}. This second Fe^{2+} in their study causes significantly more reducing power and represents a system with more dissolved Fe. Additionally, the treatments of the solvent, water, are different. Our model mixes explicit water and hydroxide with a dielectric model, C-PCM, compared to explicit hydration in vacuum in Wander et al. [38]. Although more explicit water molecules are used in the study of the ternary Fe^{2+} complex, the water may be unphysically constrained to the Fe^{2+} and carbonate because of the vacuum approach. This could influence the energy of H^+ transfer to CO_3^- because the molecule is not satisfied by any form of explicit or implicit solvation (i. e. C-PCM). This potential overestimation of the energy gain associated with PT may also affect the calculated kinetics of the PCET process. Our approach seeks to find a middle ground between a fully quantum-mechanical MD approach and a static calculation in vacuum. By using the C-PCM implicit hydration scheme in our models, in addition to a modest number of explicit water molecules, we should be able to capture more realistic system energies versus calculations conducted with explicit hydration alone. The C-PCM model allows coordinating water molecules to move within the system. This behavior results in spontaneous PT from H_2S to carbonate and H bonding of water to actinyl O in a number of the models. However, PCET to the actinyls is not observed without the manual transfer of water or bicarbonate H^+ to actinyl O.

The calculated energetics of these PT and PCET reactions with the manually-adjusted uranyl and plutonyl inner-sphere complexes with Fe^{2+} are consistent with the relative electron affinities of U^{6+} and Pu^{6+} [79]. Notably, our systems show that protonation of one or two carbonate groups alone does not result in ET as was observed by Wander et al. [38]; only PT to the actinyl O can cause reduction of An^{6+} to An^{5+}. This finding is supported by our previous work on the reaction of $[PuO_2(OH)_2(H_2O)_3]^0$ with $[Fe(OH)_2(H_2O)_4]^0$ where PT to actinyl O from coordinating water resulted in reduction of Pu^{6+} to Pu^{5+} by Fe^{2+} [41]. The computational approach taken here should be capable of capturing a PCET process if one is energetically favorable. Since the vast majority of the tested PT pathways do not appear to be energetically favorable it is understandable that our optimizations did not spontaneously arrive at the post-PT and/or post-ET atomic and electronic configurations.

The formation of inner-sphere complexes of $[Fe(OH)_2(H_2O)_4]^0$ and $[H_2S(H_2O)_6]^0$ with AnO_2^+ and AnO_2^{2+} tricarbonate complexes is slow for a majority of the tested reactions. Some reactions even show prohibitively-large E_a values for inner-sphere complex formation. Reactions with energy barriers larger than ~100 kJ/mol have typically very slow kinetics of inner-sphere complex formation and increase concentration of the outer-sphere complex over time, similar to the course of the ISC curve over time in Figure 6a. The approach of HS^- and the reorganization of tightly-bound OH^- around Fe^{2+} as the An-reductant distance is decreased results in energetically-unfavorable geometries corresponding to the transition states between the energy minima of the outer- and inner-sphere complexes. Since the inner-sphere complexes represent the global energy minimum in all cases except for UO_2^{2+} reaction with H_2S, it is possible that the E_a could be lower for a number of these transitions. Models with more explicit water (ideally a quantum-mechanical MD calculation with more H_2O and a surrounding dielectric fluid which is computationally intensive) would likely be able to lessen the impact of one or two H bonds breaking during a given distance step.

As such, it is important to consider the kinetic parameters presented in Table 3 as values that represent only the specific reaction path tested in this study and corresponding structural response. The behavior of the explicit solvent molecules in the models is semi-random and will be different if the trajectory of the incoming reactant is changed. Performing replicate distance series calculations and averaging the results may be a way to work towards a more statistically-relevant and robust measure of the E_a for a given reaction, but that would require significant computational effort that is beyond the scope of this study.

Direct evaluation of the calculated parameters in this study with other computational or experimental data is a challenge as no data for these reactions of uranyl, neptunyl, and plutonyl exist at this time. The rates of formation and conversion between different outer- and inner-sphere complexes can be determined analytically, but traditional colorimetric methods require that the different analyte complexes are distinctly colored [80, 81]. These methods can be applied to a range of different metal complexes, but are generally more appropriate for highly-conjugated organic ligands that absorb in the visible spectrum. As time-resolved infrared and X-ray spectroscopy methods develop further, it may eventually be possible to characterize the formation of different complexes *in situ* based on bond distances, vibrational modes, and oxidation state changes [82, 84]. However, if the time scales of these reactions are very fast it may be beyond the resolution of these approaches and necessitate computational treatment.

The results of this study support the understanding that actinyl tricarbonate complexes are more resistant to reduction than water or hydrolysis complexes [37]. This agrees with an array of experimental studies that have investigated the ability of actinyl molecules to participate in sorption and heterogeneous redox reactions on mineral surfaces. The formation of actinyl tricarbonate complexes is dependent on a sufficiently high CO_3^{2-} concentrations and pH >8. At this pH, many minerals are very close to or above their points of zero charge [85, 86]. While sorption of positively-charged actinyls and their complexes in carbonate-free solutions is strong at elevated pH, the opposite effect is observed when negatively-charged carbonate complexes are present. Increasing pH and carbonate concentrations diminish the formation of various ternary actinyl-carbonate inner-sphere complexes on a wide range of mineral surfaces including Fe [35, 39, 40, 87] and Mn [88] (oxyhydr)oxides, and silicate minerals (including clays) [89, 90]. Decreased propensity for inner-sphere complex formation also lowers the likelihood of heterogeneous ET reactions that can reduce actinides to their less-soluble An^{4+} state on minerals containing electron donors like Fe^{2+} [91, 92]. Based on the calculations of homogeneous reactions in this study, it appears that carbonate complexation also serves to protect these species even if reductants like Fe^{2+} and H_2S are present as dissolved components in solution. With minimal sorption to mineral surfaces and slow kinetics of inner-sphere complex formation and PCET, most AnO_2^+ and AnO_2^{2+} tricarbonate complexes likely remain highly-mobile species at elevated pH conditions.

5 Conclusions

This work indicates that homogeneous electron transfer (ET) from Fe^{2+} and H_2S to AnO_2^{2+} and AnO_2^+ tricarbonate complexes is unlikely to proceed without the transfer of a proton (or two) to the actinyl O atoms. While carbonate is known to impede the reduction of uranyl in heterogeneous reactions at electrode surfaces, it was expected that there would be some evidence for ET if the reductant is brought into close enough proximity to the actinyl. Neptunyl and plutonyl, which preferentially form monovalent actinyl species in most aqueous settings [93, 94], are stabilized as An^{6+} in the presence of these two reductants. The reduction of An^{5+} to An^{4+} involves significant reorganization of the local coordination environment (increase in CN from 5 to 7 or 8) and it has been calculated that this process is energetically-unfavorable and will not proceed with Fe^{2+} as the electron donor [31, 32, 38]. Our calculations support and provide further evidence for the understanding that carbonate can stabilize higher-valent actinides and prevent reduction to the more insoluble An^{4+} state, particularly under higher pH conditions where sorption to mineral surfaces is less prevalent.

The calculated rates of collision (encounter complex formation) and transition from outer- to inner-sphere complex reveal that the formation of outer-sphere complexes is energetically-favorable and the rate is largely dependent on the diffusion velocities of both reactants and the concentration of the less abundant species. Even at very low actinyl concentrations (nM and pM) the reaction to form the outer-sphere complex between an actinyl tricarbonates and $[H_2S(H_2O)_6]^0$ or $[Fe(OH)_2(H_2O)_4]^0$ is expected to proceed rapidly with nearly all of the actinyl species consumed over a time period on the order of seconds. After that, the conversion to the inner-sphere complex, which should increase the likelihood of ET, is highly-sensitive to changes in the H bonding environment of the first solvation shell. Differences in the H bonding networks between H_2O, OH^-, and (bi)carbonate yield a wide range of E_a values for different reactant pairs. The variability in the calculated energy barriers appears to be

somewhat random and dependent on the trajectory of just a few water molecules in the system.

The results of this study highlight the need for further investigation and testing of the appropriate computational approaches for calculating reactions in which proton-coupled electron transfer (PCET) may be a key pathway for reduction. In some cases, a geometry optimization calculation may capture PCET without specific user inputs nudging the geometry towards this reaction pathway [41]. In other cases, like the calculations presented here, manual placement of H^+ on the actinyl O atoms is required for reduction of An^{6+} to An^{5+} to occur. No reduction is observed spontaneously in any of the reactions of uranyl, neptunyl, or plutonyl tricarbonate complexes when hydration is modeled with explicit water and C-PCM. Exploration of different post-PT structures indicate that this process can yield thermodynamically-favorable one electron reduction of An^{6+} to An^{5+}; however, not all pathways are energetically favorable or accompanied by ET. Simulating an electric field to pull electron density towards the actinyl molecule from the reductant yielded ET without PT, but the field strength required is relatively high.

In future work, it may be beneficial to consider how the computational methodology may be altered to permit more solvent molecules to be included explicitly in the model. These sort of calculations may be an excellent candidate for the use of a hybrid quantum mechanics/molecular mechanics (QM/MM) approach that allows a certain subset of the atoms or molecules to be treated at the more robust quantum-mechanical level, while the rest of the system, perhaps including several higher order shells of explicit solvent molecules, is treated with a reactive atomistic reactive force field approach that allows for donating and accepting protons [95]. In this way, the redox process between a given reactant pair could be explored in detail while including a large number of explicit solvent molecules that provide a buffer for the energy changes associated with reorganization of a H bonding network. Having a large number of solvent molecules available around, for example, the actinyl tricarbonate complex may also aid the system's ability to capture PCET pathways that are not observed in our calculations, as proton donors would be nearby and the improbable "hopping" of a proton from a bicarbonate or an Fe^{2+}-coordinating water molecule would not be required.

Overall, much of the chemical behavior of actinyl (tri)carbonate complexes remains to be explored in both experimental and computational settings. Adsorption of these complexes to a range of different mineral surfaces under different solution conditions has been studied [35, 88, 90, 96–98]. Broadly, it can be said that at high pH, the negatively-charged bi- and tricarbonate complexes of actinyls are less likely to sorb to a wide range of mineral phases with negatively-charged surfaces (i. e. above their points of zero charge). Heterogeneous reactions of these complexes dominate at lower pH where they adsorb, strongly in some cases, to mineral surfaces which may contain possible electron donors like Mn^{2+} and Fe^{2+} [36, 91, 99, 100]. The homogeneous reactions of the actinyl carbonate complexes appear to require the PCET mechanism in order for reduction to occur [31, 38]. This process is likely more challenging at higher pH conditions where systems are relatively proton-poor.

The calculated reaction kinetics presented here suggest that inner-sphere complex formation between actinyls and Fe^{2+} and H_2S, and PCET, is kinetically and, in some cases, thermodynamically inhibited by carbonate complexation. Our calculated kinetic parameters represent ΔE of different reactions, but a subset of frequency calculations verify that the E_a values derived from the electronic energy trajectories are within 5–10 % of ΔG. In a number of reactions, the transition from outer- to inner-sphere complex appears to be the rate-limiting step for the homogeneous reduction of these actinide species. With this in mind, these reactions may be good candidates for receiving assistance from a mediating mineral surface. In the future, a modified version of the computational approach used in this study could be used to investigate the role of a mineral surface in lowering energy barriers associated with decomplexation, decarbonation, and/or dehydration during the formation of inner-sphere complexes. While eventually it may be feasible to perform quantum-mechanical molecular-dynamics calculations on large systems with many solvent molecules, for now applying the sequential reactant distance series approach of this work to heterogeneous reactions could be a relatively straightforward means of learning more about these processes on a fundamental level. Combining these calculations with Marcus Theory, as has been applied to homogeneous [31, 38, 77] and heterogeneous [50, 51, 101] reactions of actinide complexes, would allow for a complete description of the kinetics of these processes. These approaches warrant further testing and application to actinide complexes and other contaminants of interest and can serve to support experimental findings and their interpretation.

6 Supplementary information

The Supplementary Information document includes an example input Gaussian input file including the keywords (header) and z-matrix coordinate set up. The SI also contains cartesian coordinates for complex structures shown in

Figures 5a–c and 8a, b. Tables S1 and S2 present the calculated reaction energies for various proton transfer pathways described in Section 3.5 for uranyl and plutonyl, respectively.

Acknowledgements: This research was supported by funding from the U.S. Department of Energy's (DOE) Office of Science, Office of Basic Energy Sciences (BES), Chemical Sciences, Geosciences, & Biosciences (CSGB) Division for the topics of Heavy Element Chemistry and Geoscience (grant number DE-FG02-06ER15783, Funder Id: http://dx.doi.org/10.13039/100006151). The calculations for this study were carried out in part on the Flux high-performance computing cluster managed by University of Michigan Advanced Research Computing Technology Services (ARC-TS). The authors would like to acknowledge two anonymous reviewers for their comments and suggestions that improved the quality of this manuscript and thank Thomas Albrecht-Schmitt for his editorial handling of the submission.

References

1. Maher, K., Bargar, J. R., Brown, G. E.: Environmental speciation of actinides. Inorg. Chem. **52**, 7 (2013).
2. Geckeis, H., Lutzenkirchen, J., Polly, R., Rabung, T., Schmidt, M.: Mineral-water interface reactions of actinides. Chem. Rev. **113**, 2 (2013).
3. Szabo, Z., Toraishi, T., Vallet, V., Grenthe, I.: Solution coordination chemistry of actinides: thermodynamics, structure and reaction mechanisms. Coord. Chem. Rev. **250**, 7 (2006).
4. Newsome, L., Morris, K., Lloyd, J. R.: The biogeochemistry and bioremediation of uranium and other priority radionuclides. Chem. Geol. **363**, 164 (2014).
5. Neck, V., Kim, J. I.: Solubility and hydrolysis of tetravalent actinides. Radiochim. Acta **89**, 1 (2001).
6. Clark, D. L., Hobart, D. E., Neu, M. P.: Actinide carbonate complexes and their importance in actinide environmental chemistry. Chem. Rev. **95**, 1 (1995).
7. Choppin, G. R.: Actinide speciation in the environment. J. Radioanal. Nucl. Chem. **273**, 3 (2007).
8. Djogic, R., Sipos, L., Branica, M.: Characterization of uranium(VI) in seawater. Limnol. Oceanogr. **31**, 5 (1986).
9. Docrat, T. I., Mosselmans, J. F. W., Charnock, J. M., Whiteley, M. W., Collison, D., Livens, F. R., Jones, C., Edmiston, M. J.: X-ray absorption spectroscopy of tricarbonatodioxouranate(V), $UO_2(CO_3)_3^{5-}$, in aqueous solution. Inorg. Chem. **38**, 8 (1999).
10. Dong, W. M., Brooks, S. C.: Determination of the formation constants of ternary complexes of uranyl and carbonate with alkaline earth metals (Mg^{2+}, Ca^{2+}, Sr^{2+}, and Ba^{2+}) using anion exchange method. Environ. Sci. Technol. **40**, 15 (2006).
11. Geipel, G., Amayri, S., Bernhard, G.: Mixed complexes of alkaline earth uranyl carbonates: a laser-induced time-resolved fluorescence spectroscopic study. Spectrochim. Acta A **71**, 1 (2008).
12. Geipel, G., Bernhard, G., Brendler, V., Nitsche, H.: Complex formation between UO_2^{2+} and CO_3^{2-}: studied by laser-induced photoacoustic spectroscopy (LIPAS). Radiochim. Acta **82**, 59 (1998).
13. Kato, Y., Kimura, T., Yoshida, Z., Nitani, N.: Carbonate complexation of neptunyl(VI) ion. Radiochim. Acta **82**, 63 (1998).
14. Gagliardi, L., Roos, B. O.: Coordination of the neptunyl ion with carbonate ions and water: a theoretical study. Inorg. Chem. **41**, 5 (2002).
15. Ikeda-Ohno, A., Tsushima, S., Takao, K., Rossberg, A., Funke, H., Scheinost, A. C., Bernhard, G., Yaita, T., Hennig, C.: Neptunium carbonato complexes in aqueous solution: an electrochemical, spectroscopic, and quantum chemical study. Inorg. Chem. **48**, 24 (2009).
16. de Jong, W. A., Apra, E., Windus, T. L., Nichols, J. A., Harrison, R. J., Gutowski, K. E., Dixon, D. A.: Complexation of the carbonate, nitrate, and acetate anions with the uranyl dication: density functional studies with relativistic effective core potentials. J. Phys. Chem. A **109**, 50 (2005).
17. Grenthe, I., Ferri, D., Salvatore, F., Riccio, G.: Studies on metal carbonate equilibria. Part 10. A solubility study of the complex formation in uranium(VI)-water-carbon dioxide (g) system at 25 °C. J. Chem. Soc. – Dalton T. **11**, 2439 (1984). dx.doi.org/10.1039/DT9840002439.
18. De Pablo, J., Casas, I., Gimenez, J., Molera, M., Rovira, M., Duro, L., Bruno, J.: The oxidative dissolution mechanism of uranium dioxide. I. The effect of temperature in hydrogen carbonate medium. Geochim. Cosmochim. Acta **63**, 19 (1999).
19. Zhou, P., Gu, B. H.: Extraction of oxidized and reduced forms of uranium from contaminated soils: effects of carbonate concentration and pH. Environ. Sci. Technol. **39**, 12 (2005).
20. Hua, B., Deng, B. L.: Reductive immobilization of uranium(VI) by amorphous iron sulfide. Environ. Sci. Technol. **42**, 23 (2008).
21. Bernhard, G., Geipel, G., Reich, T., Brendler, V., Amayri, S., Nitsche, H.: Uranyl(VI) carbonate complex formation: validation of the $Ca_2UO_2(CO_3)_3$(aq.) species. Radiochim. Acta **89**, 8 (2001).
22. Stewart, B. D., Mayes, M. A., Fendorf, S.: Impact of uranyl-calcium-carbonato complexes on uranium(VI) adsorption to synthetic and natural Sediments. Environ. Sci. Technol. **44**, 3 (2010).
23. Duro, L., Missana, T., Ripoll, S., Grive, M., Bruno, J.: Modelling of Pu sorption onto the surface of goethite and magnetite as steel corrosion products. In: V. M. Oversby, L. O. Werme (Eds.), Scientific Basis for Nuclear Waste Management XXVII (2004), MRS Proceedings, Materials Research Society, Warrendale, PA, USA, vol. 807, p. 659–664.
24. Pearce, C. I., Rosso, K. M., Pattrick, R. A. D., Felmy, A. R.: Impact of iron redox chemistry on nuclear waste disposal. In: I. A. M. Ahmed, K. A. Hudson-Edwards (Eds.), Redox-Reactive Minerals: Properties, Reactions and Applications in Clean Technologies (2017), European Mineralogical Union, Jena, Germany, vol. 17, p. 229–272.
25. Dodge, C. J., Francis, A. J., Gillow, J. B., Halada, G. P., Eng, C., Clayton, C. R.: Association of uranium with iron oxides typically formed on corroding steel surfaces. Environ. Sci. Technol. **36**, 16 (2002).
26. Wersin, P., Hochella, M. F., Persson, P., Redden, G., Leckie, J. O., Harris, D. W.: Interaction between aqueous uranium(VI) and sulfide minerals – spectroscopic evidence for soption and reduction. Geochim. Cosmochim. Acta **58**, 13 (1994).
27. Renock, D., Mueller, M., Yuan, K., Ewing, R. C., Becker, U.: The energetics and kinetics of uranyl reduction on pyrite, hematite,

and magnetite surfaces: a powder microelectrode study. Geochim. Cosmochim. Acta **118** (2013).
28. Moyes, L. N., Jones, M. J., Reed, W. A., Livens, F. R., Charnock, J. M., Mosselmans, J. F. W., Hennig, C., Vaughan, D. J., Pattrick, R. A. D.: An X-ray absorption spectroscopy study of neptunium(V) reactions with mackinawite (FeS). Environ. Sci. Technol. **36**, 2 (2002).
29. Scott, T. B., Tort, O. R., Allen, G. C.: Aqueous uptake of uranium onto pyrite surfaces; reactivity of fresh versus weathered material. Geochim. Cosmochim. Acta **71**, 21 (2007).
30. Hua, B., Xu, H. F., Terry, J., Deng, B. L.: Kinetics of uranium(VI) reduction by hydrogen sulfide in anoxic aqueous systems. Environ. Sci. Technol. **40**, 15 (2006).
31. Collins, R. N., Rosso, K. M.: Mechanisms and rates of U(VI) reduction by Fe(II) in homogeneous aqueous solution and the role of U(V) disproportionation. J. Phys. Chem. A **121**, 35 (2017).
32. Odoh, S. O., Schreckenbach, G.: Theoretical study of the structural properties of plutonium(IV) and (VI) complexes. J. Phys. Chem. A **115**, 48 (2011).
33. Wang, Z., Wagnon, K. B., Ainsworth, C. C., Liu, C., Rosso, K. M., Fredrickson, J. K.: A spectroscopic study of the effect of ligand complexation on the reduction of uranium(VI) by anthraquinone-2,6-disulfonate (AH_2DS). Radiochim. Acta **96**, 9 (2008).
34. Yan, S., Hua, B., Bao, Z. Y., Yang, J., Liu, C. X., Deng, B. L.: Uranium(VI) removal by nanoscale zerovalent iron in anoxic batch systems. Environ. Sci. Technol. **44**, 20 (2010).
35. Duff, M. C., Amrhein, C.: Uranium(VI) adsorption on goethite and soil in carbonate solutions. Soil Sci. Soc. Am. J. **60**, 5 (1996).
36. Barnett, M. O., Jardine, P. M., Brooks, S. C., Selim, H. M.: Adsorption and transport of uranium(VI) in subsurface media. Soil Sci. Soc. Am. J. **64**, 3 (2000).
37. Morris, D. E.: Redox energetics and kinetics of uranyl coordination complexes in aqueous solution. Inorg. Chem. **41**, 13 (2002).
38. Wander, M. C. F., Kerisit, S., Rosso, K. M., Schoonen, M. A. A.: Kinetics of triscarbonato uranyl reduction by aqueous ferrous iron: a theoretical study. J. Phys. Chem. A **110**, 31 (2006).
39. Kohler, M., Honeyman, B. D., Leckie, J. O.: Neptunium(V) sorption on hematite (α-Fe_2O_3) in aqueous suspension: the effect of CO_2. Radiochim. Acta **85**, 1 (1999).
40. Wazne, M., Korfiatis, G. P., Meng, X. G.: Carbonate effects on hexavalent uranium adsorption by iron oxyhydroxide. Environ. Sci. Technol. **37**, 16 (2003).
41. Bender, W. M., Becker, U.: Determining the kinetics of discrete aqueous redox reaction sub-steps using computational methods: application to reactions of plutonyl ($PuO_2^{+/2+}$) with Fe^{2+}, Fe^{3+}, and hydroxyl radical (•OH). Am. J. Sci. **318**, 893 (2018).
42. Frisch, M. J., Trucks, G. W., Schelgel, H. B., Scuseria, G. E., Robb, M. A., Cheeseman, J. R., Scalmani, G., Barone, V., Petersson, G. A., Nakatsuji, H., Li, X., Caricato, M., Marenich, A., Bloino, J., Janesko, B. G., Gomperts, R., Mennucci, B., Hratchian, H. P., Ortiz, J. V., Izmaylov, A. F., Sonnenber, J. L., Williams-Young, D., Ding, F., Lipparini, F., Egidi, F., Goings, J., Peng, B., Petrone, A., Henderson, T., Ranasinghe, D., Zakrzewski, V. G., Gao, J., Rega, N., Zheng, G., Liang, W., Hada, M., Ehara, M., Toyota, K., Fukuda, R., Hasegawa, J., Ishida, M., Nakajima, T., Honda, Y., Kitao, O., Nakai, H., Vreven, T., Throssell, K., Montgomery, J., J. A., Peralta, J. E., Ogliaro, F., Bearpark, M., Heyd, J. J., Brothers, E., Kudin, K. N., Staroverov, V. N., Keith, T., Kobayashi, R., Normand, J., Raghavachari, K., Rendell, A., Burant, J. C., Iyengar, S. S., Tomasi, J., Cossi, M., Millam, J. M., Klene, M., Adamo, C., Cammi, R., Ochterski, J. W., Martin, R. L., Morokuma, K., Farkas, O., Foresman, J. B., Fox, D. J.: Gaussian 09, Revision A.02, Gaussian, Inc., Wallingford, CT (2016).
43. Becke, A. D.: Density-functional thermochemistry. III. The role of exact exchange. J. Chem. Phys. **98**, 7 (1993).
44. Lee, C. T., Yang, W. T., Parr, R. G.: Development of the Colle-Salvetti correlation-energy formula into a functional of the electron-density. Phys. Rev. B **37**, 2 (1988).
45. Wadt, W. R., Hay, P. J.: Ab initio effective core potentials for molecular calculations – potentials for main group elements Na to Bi. J. Chem. Phys. **82**, 284 (1985).
46. Dunning Jr., T. H., Hay, P. J.: Gaussian basis sets for molecular calculations. In: H. F. Schaefer (Ed.), Methods of Electronic Structure Theory, 1 ed., (1977), Springer US, New York, p. 1–27.
47. Dunning, T. H.: Gaussian basis sets for use in correlated molecular calculations. I. The atoms boron through neon and hydrogen. J. Chem. Phys. **90** (1989).
48. Dolg, M., Wedig, U., Stoll, H., Preuss, H.: Energy-adjusted *ab initio* pseudopotentials for the first row transition elements. J. Chem. Phys. **86**, 2 (1987).
49. Küchle, W., Dolg, M., Stoll, H., Preuss, H.: Energy-adjusted pseudopotentials for the actinides. Parameter sets and test calculations for thorium and thorium monoxide. J. Chem. Phys. **100**, 10 (1994).
50. Taylor, S. D., Marcano, M. C., Becker, U.: A first principles investigation of electron transfer between Fe(II) and U(VI) on insulating Al- vs. semiconducting Fe-oxide surfaces via the proximity effect. Geochim. Cosmochim. Acta **197**, 305 (2017).
51. Taylor, S. D., Marcano, M. C., Rosso, K. M., Becker, U.: An experimental and ab initio study on the abiotic reduction of uranyl by ferrous iron. Geochim. Cosmochim. Acta **156**, 154 (2015).
52. Kerisit, S., Rosso, K. M.: Computer simulation of electron transfer at hematite surfaces. Geochim. Cosmochim. Acta **70**, 8 (2006).
53. Feller, D.: The role of databases in support of computational chemistry calculations. J. Comput. Chem. **17**, 13 (1996).
54. Schuchardt, K. L., Didier, B. T., Elsethagen, T., Sun, L., Gurumoorthi, V., Chase, J., Li, J., Windus, T. L.: Basis set exchange: a community database for computational sciences. J. Chem. Inf. Model. **47**, 3 (2007).
55. Bader, R. F. W., Anderson, S. G., Duke, A. J.: Quantum topology of molecular charge distributions. 1. J. Am. Chem. Soc. **101**, 6 (1979).
56. Bader, R. F. W., Nguyendang, T. T., Tal, Y.: Quantum topology of molecular charge distributions. II. Molecular structure and its change. J. Chem. Phys. **70**, 9 (1979).
57. Reed, A. E., Weinhold, F.: Natural localized molecular orbitals. J. Chem. Phys. **83**, 4 (1985).
58. Reed, A. E., Weinstock, R. B., Weinhold, F.: Natural population analysis. J. Chem. Phys. **83**, 2 (1985).
59. Ikeda, A., Hennig, C., Tsushima, S., Takao, K., Ikeda, Y., Scheinost, A. C., Bernhard, G.: Comparative study of uranyl(VI) and -(V) carbonato complexes in an aqueous solution. Inorg. Chem. **46**, 10 (2007).
60. Kato, Y., Meinrath, G., Kimura, T., Yoshida, Z.: A study of U(VI) hydrolysis and carbonate complexation by time-resolved laser-induced fluorescence spectroscopy (TRLFS). Radiochim. Acta **64**, 2 (1994).

61. Kerisit, S., Liu, C. X.: Molecular simulation of the diffusion of uranyl carbonate species in aqueous solution. Geochim. Cosmochim. Acta **74**, 17 (2010).
62. Klamt, A., Moya, C., Palomar, J.: A comprehensive comparison of the IEFPCM and SS(V)PE continuum solvation methods with the COSMO approach. J. Chem. Theory Comput. **11**, 9 (2015).
63. Tsushima, S., Wahlgren, U., Grenthe, I.: Quantum chemical calculations of reduction potentials of AnO_2^{2+}/AnO_2^{+} (An = U, Np, Pu, Am) and Fe^{3+}/Fe^{2+} couples. J. Phys. Chem. A **110**, 29 (2006).
64. Priest, C., Tian, Z. Q., Jiang, D. E.: First-principles molecular dynamics simulation of the $Ca_2UO_2(CO_3)_3$ complex in water. Dalton T. **45**, 24 (2016).
65. Tomasi, J., Mennucci, B., Cammi, R.: Quantum mechanical continuum solvation models. Chem. Rev. **105**, 8 (2005).
66. Cossi, M., Rega, N., Scalmani, G., Barone, V.: Energies, structures, and electronic properties of molecules in solution with the C-PCM solvation model. J. Comp. Chem. **24**, 6 (2003).
67. Barone, V., Cossi, M.: Quantum calculation of molecular energies and energy gradients in solution by a conductor solvent model. J. Phys. Chem. A **102**, 1995 (1998).
68. Haimour, N., Sandall, O. C.: Molecular diffusivity of hydrogen sulfide in water. J. Chem. Eng. Data **29**, 1 (1984).
69. Lide, D. R., Kehiaian, H. V.: CRC Handbook of Thermophysical and Thermochemical Data. CRC Press, Inc., Boca Raton (1994), p. 518.
70. Kerisit, S., Liu, C. X.: Diffusion and adsorption of uranyl carbonate species in nanosized mineral fractures. Environ. Sci. Technol. **46**, 3 (2012).
71. Kraus, K. A., Nelson, F.: Chemistry of aqueous uranium(V) solutions. II. Reaction of uranium pentachloride with water. Thermodynamic stability of UO_2^{+}. Potential of U(IV)/(V), U(IV)/(VI) and U(V)/U(VI) couples. J. Am. Chem. Soc. **71**, 7 (1949).
72. Kraus, K. A., Nelson, F., Johnson, G. L.: Chemistry of aqueous uranium(V) solutions. I. Preparation and properties. Analogy between uranium(V), neptunium(V) and plutonium(V). J. Am. Chem. Soc. **71**, 7 (1949).
73. Glicksman, M. E.: Diffusion in Solids: Field Theory, Solid-State Principles, and Applications. John Wiley & Sons, New York (1999), p. 498.
74. Reich, M., Ewing, R. C., Ehlers, T. A., Becker, U.: Low-temperature anisotropic diffusion of helium in zircon: implications for zircon (U-Th)/He thermochronometry. Geochim. Cosmochim. Acta **71**, 12 (2007).
75. Grimme, S., Antony, J., Ehrlich, S., Krieg, H.: A consistent and accurate ab initio parametrization of density functional dispersion correction (DFT-D) for the 94 elements H-Pu. J. Chem. Phys. **132**, 15 (2010).
76. Grimme, S., Ehrlich, S., Goerigk, L.: Effect of the damping function in dispersion corrected density functional theory. J. Comp. Chem. **32**, 7 (2011).
77. Privalov, T., Schimmelpfennig, B., Wahlgren, U., Grenthe, I.: Reduction of uranyl(VI) by iron(II) in solutions: an ab initio study. J. Phys. Chem. A **107**, 4 (2003).
78. Car, R., Parrinello, M.: Unified approach for molecular-dynamics and density functional theory. Phys. Rev. Lett. **55**, 22 (1985).
79. Steele, H. M., Guillaumont, D., Moisy, P.: Density functional theory calculations of the redox potentials of actinide(VI)/actinide(V) couple in water. J. Phys. Chem. A **117**, 21 (2013).
80. Taube, H.: Electron Transfer Reactions of Complex Ions in Solution. Academic Press, New York (1970), p. 103.
81. Marcus, R. A., Sutin, N.: Electron transfers in chemistry and biology. BBA-Bioergetics **811**, 3 (1985).
82. Guckel, K., Rossberg, A., Müller, K., Brendler, V., Bernhard, G., Foerstendorf, H.: Spectroscopic identification of binary and ternary surface complexes of Np(V) on gibbsite. Environ. Sci. Technol. **47**, 24 (2013).
83. Müller, K., Groschel, A., Rossberg, A., Bok, F., Franzen, C., Brendler, V., Foerstendorf, H.: In situ spectroscopic identification of neptunium(V) inner-sphere complexes on the hematite-water interface. Environ. Sci. Technol. **49**, 4 (2015).
84. Zhu, M. Q., Legg, B., Zhang, H. Z., Gilbert, B., Ren, Y., Banfield, J. F., Waychunas, G. A.: Early stage formation of iron oxyhydroxides during neutralization of simulated acid mine drainage solutions. Environ. Sci. Technol. **46**, 15 (2012).
85. Parks, G. A., de Bruyn, P. L.: The zero point charge of oxides. J. Phys. Chem. **66**, 6 (1962).
86. Pechenyuk, S. I.: The use of the pH at the point of zero charge for characterizing the properties of oxide hydroxides. Russ. Chem. Bull. **48**, 6 (1999).
87. Tinnacher, R. M., Zavarin, M., Powell, B. A., Kersting, A. B.: Kinetics of neptunium(V) sorption and desorption on goethite: an experimental and modeling study. Geochim. Cosmochim. Acta **75**, 21 (2011).
88. Duff, M. C., Hunter, D. B., Triay, I. R., Bertsch, P. M., Reed, D. T., Sutton, S. R., Shea-Mccarthy, G., Kitten, J., Eng, P., Chipera, S. J., Vaniman, D. T.: Mineral associations and average oxidation states of sorbed Pu on tuff. Environ. Sci. Technol. **33**, 13 (1999).
89. Bertetti, F. P., Pabalan, R. T., Almendarez, M. G.: Studies of neptunium^{V} sorption on quartz, clinoptilolite, montmorillonite, and α-alumina. In: E. A. Jenne (Ed.), Adsorption of Metals by Geomedia (1998), Academic Press, San Diego, p. 132–149.
90. Catalano, J. G., Brown, G. E.: Uranyl adsorption onto montmorillonite: evaluation of binding sites and carbonate complexation. Geochim. Cosmochim. Acta **69**, 12 (2005).
91. Begg, J. D., Edelman, C., Zavarin, M., Kersting, A. B.: Sorption kinetics of plutonium (V)/(VI) to three montmorillonite clays. Appl. Geochem. **96** (2018).
92. Zhao, P. H., Begg, J. D., Zavarin, M., Tumey, S. J., Williams, R., Dai, Z. R. R., Kips, R., Kersting, A. B.: Plutonium(IV) and (V) sorption to goethite at sub-femtomolar to micromolar concentrations: redox transformations and surface precipitation. Environ. Sci. Technol. **50**, 13 (2016).
93. Vallet, V., Macak, P., Wahlgren, U., Grenthe, I.: Actinide chemistry in solution, quantum chemical methods and models. Theor. Chem. Acc. **115**, 2 (2006).
94. Silva, R. J., Nitsche, H.: Actinide environmental chemistry. Radiochim. Acta **70**, 1 (1995).
95. Tirler, A. O., Hofer, T. S.: Structure and dynamics of the uranyl tricarbonate complex in aqueous solution: insights from quantum mechanical charge field molecular dynamics. J. Phys. Chem. B **118**, 45 (2014).
96. Bargar, J. R., Reitmeyer, R., Davis, J. A.: Spectroscopic confirmation of uranium(VI)-carbonato adsorption complexes on hematite. Environ. Sci. Technol. **33**, 14 (1999).
97. Ho, C. H., Miller, N. H.: Adsorption of uranyl species from bicarbonate solution onto hematite particles. J. Colloid Interf. Sci. **110**, 1 (1986).

98. Bargar, J. R., Reitmeyer, R., Lenhart, J. J., Davis, J. A.: Characterization of U(VI)-carbonato ternary complexes on hematite: EXAFS and electrophoretic mobility measurements. Geochim. Cosmochim. Acta **64**, 16 (2000).
99. Qafoku, N. P., Zachara, J. M., Liu, C. X., Gassman, P. L., Qafoku, O. S., Smith, S. C.: Kinetic desorption and sorption of U(VI) during reactive transport in a contaminated Hanford sediment. Environ. Sci. Technol. **39**, 9 (2005).
100. Singer, D. M., Chatman, S. M., Ilton, E. S., Rosso, K. M., Banfield, J. F., Waychunas, G. A.: U(VI) sorption and reduction kinetics on the magnetite (111) surface. Environ. Sci. Technol. **46**, 7 (2012).
101. Taylor, S. D., Becker, U., Rosso, K. M.: Electron transfer pathways facilitating U(VI) reduction by Fe(II) on Al- vs. Fe-oxides. J. Phys. Chem. C **121**, 36 (2017).

Supplementary Material: The online version of this article offers supplementary material (https://doi.org/10.1515/ract-2018-3083).